Available online at www.sciencedirect.com
SCIENCE DIRECT®
International Journal of Solids and Structures 42 (2005) 2361–2379
INTERNATIONAL JOURNAL OF SOLIDS and STRUCTURES
www.elsevier.com/locate/ijsolstr

Generalized plane strain finite element model for the analysis of elastoplastic composites

Alberto Taliercio *

Department of Structural Engineering, Politecnico di Milano, Piazza Leonardo da Vinci 32, I-20133 Milan, Italy

Received 17 December 2003; received in revised form 23 September 2004

Abstract

A numerical model is presented, based on the finite element method in its displacement formulation, aimed at the analysis of the representative volume element (RVE) of composites reinforced by a regular array of long, parallel fibers, subjected to any 3-D macroscopic stress or strain state. Special finite elements are formulated, which are capable of describing three-dimensional deformation modes associated with strain fields invariant along the fiber axis. Periodicity boundary conditions at the sides of the RVE complete the kinematic formulation. The model is applied to metal–matrix composites, assuming an elastic–perfectly plastic behaviour for both phases; the compatibility matrix of the finite elements is modified, according to proposals of other authors, to avoid locking phenomena near the fully plastic range. Some numerical applications are shown to illustrate the possibility of employing the model to predict the macroscopic response of metal–matrix composites in the non-linear field and up to failure. Comparisons with analytical and experimental results available in the literature testify the reliability of the model estimates.

Keywords: Fiber-reinforced composites; Metal–matrix composites; Plasticity; Finite elements; Homogenization

1. Introduction

Predicting the global (or average, or macroscopic) mechanical response of fiber-reinforced composites (FRCs) starting from the knowledge of the local (or microscopic) properties of their constituents is a goal that many researchers have set themselves in the last decades. This information is of great importance, for instance, when the materials to be employed in the design of a new composite with prescribed stiffness (or strength) properties have to be selected.

* Tel.: +39 2 23994241; fax: +39 2 2399 4220.
E-mail address: alberto.taliercio@polimi.it

0020-7683/$ - see front matter © 2004 Published by Elsevier Ltd.
doi:10.1016/j.ijsolstr.2004.09.030

Historically, the first works regarding the prediction of the macroscopic properties of heterogeneous media, including FRCs, covered the linear elastic range, and essentially aimed at giving estimates for the average elasticities in (semi-)analytical form. Among these, considerable diffusion have found the bounds formulated by Hashin and Shtrikman (1963) on a variational basis; the concentric cylinder assemblage model proposed by Hashin and Rosen (1964); the methods exploiting the concept of Eshelby's tensor (Eshelby, 1957), such as the self-consistent method (Hill, 1965) or the Mori–Tanaka method, revisited by Benveniste (1987); and the method of cells for periodically reinforced composites (see e.g. Aboudi, 1991, for a comprehensive treatment).

Most of these methods were later extended to predict the non-linear macroscopic behaviour of composites. For instance, the self-consistent method was extended by Dvorak and Bahei-El-Din (1979) to the plastic range. Also, the method of cells was applied by Pindera and Aboudi (1988) to predict the initial yield surfaces of metal–matrix composites. Widely known is also the model proposed by Teply and Dvorak (1988) to predict the response of composites evenly reinforced by a periodic hexagonal array with elasto-plastic constituents.

Models suitable to the description of the global response of composites in presence of damage phenomena have also been formulated, incorporating both debonding processes at the fiber–matrix interface (see e.g. Ju and Lee, 2001) and delamination effects at the contact surface between different layers in multilayered laminates: see, e.g., Corigliano (2003) for a comprehensive review on computational damage and fracture methods for composites.

Many of the numerical models quoted above are based on the finite element method for the solution of the governing equations. So far, at the author's knowledge, the prediction of the non-linear behaviour of elastic–plastic composites subjected to a general state of stress has mostly been performed using 3-D models, which obviously makes the numerical analyses burdensome. In this paper, a finite element model is proposed, which explicitly takes advantage of the geometry of the reinforcement. Indeed, allowing for the theoretically unlimited length of the fibers in unidirectionally reinforced composites, the problem can be reduced to the analysis of any cross-section of the material, which is in a state of 'generalized plane strain', as discussed later.

The layout of the paper is as follows. In Section 2 some basic concepts are briefly reviewed regarding the theory of homogenization for heterogeneous media with periodic structure, which is the starting point for the development of many micromechanically-based theoretical models for composites. Section 3 is devoted to the description of a finite element numerical model, which allows a representative volume element (RVE) of composite with long, parallel fibers to be analyzed by explicitly accounting for its particular geometry, as outlined above. A new type of 2-D finite elements, endowed with the 3-D kinematics of a solid in generalized plane strain conditions, is presented in Section 3.1. The kinematic conditions to be imposed at the boundary of the discretized RVE to match the periodicity of the medium are detailed in Section 3.2. Section 3.3 describes the modifications to be made to the compatibility matrix of the elements to correctly predict the ultimate strength of incompressible perfectly plastic FRCs. The effectiveness of the model is assessed in Section 4, through comparisons both with theoretical estimates of the macroscopic strength domains of MMCs subjected to multiaxial stresses (Section 4.1) and some available experimental results (Section 4.2). Finally, some remarks on the proposed model are made in Section 5, where possible future developments are also outlined.

2. An outline of homogenization theory for periodic media

It is well known that 'homogenization' is the substitution of a real heterogeneous medium with an ideal, homogeneous continuum. The properties of this medium are derived through analyses of a 'Representative Volume Element' (see e.g. Nemat-Nasser and Hori, 1993), that is, a volume that is sufficiently large to

include an effective sampling of the heterogeneous microstructure of the medium. If the heterogeneous medium consists of a matrix embedding evenly distributed inclusions of the same shape, the medium is said to be *periodic*, and a single 'unit cell' can be taken as RVE. The entire periodic medium can be seen as a collection of contiguous, equal unit cells. The computational effort to analyze this kind of RVE is greatly reduced in comparison with heterogeneous media with random inclusions.

In real composites, the arrangement of the reinforcing array is essentially random. For unidirectional composites with long fibers, the simplifying assumption is commonly made of considering fibers evenly spaced. The consequences of neglecting any randomness in the reinforcing array of metal–matrix composites (MMCs) were investigated by Brockenbrough et al. (1991). The authors considered several types of periodic packing arrangements for MMCs with continuous fibers and concluded that the results for a 'triangle-packing arrangement' satisfactorily match those of a random-packing. Accordingly, in this work, fibers are supposed to be located at the corners of equilateral triangles. A possible choice for the unit cell is a prism of unlimited length, embedding a single fiber, the cross-section of which is a regular hexagon (see Fig. 1); note that the length of the unit cell along the fiber axis, z, is immaterial.

Stresses and strains at any point of the homogenized medium (also called 'macroscopic' stresses and strains, and denoted by $\boldsymbol{\Sigma}$ and $\boldsymbol{E}$, respectively) are defined as the averages over any RVE of the corresponding local (or microscopic) quantities, $\boldsymbol{\sigma}$ and $\boldsymbol{\epsilon}$, provided that the RVE does not embed any crack or cavity (see e.g. Nemat-Nasser and Hori, 1993). Thus:

$$\boldsymbol{\Sigma} = \frac{1}{|V|}\int_V \boldsymbol{\sigma}(\boldsymbol{x})\,\mathrm{d}V; \quad \boldsymbol{E} = \frac{1}{|V|}\int_V \boldsymbol{\epsilon}(\boldsymbol{x})\,\mathrm{d}V. \tag{1}$$

Here, V is the volume of the RVE and $\boldsymbol{x}$ is any point in V.

In the case of periodic media, the microscopic fields have to fulfill suitable periodicity conditions ensuring continuity of boundary tractions ($\boldsymbol{t}$) and displacements ($\boldsymbol{u}$) across adjacent cells (see e.g. Suquet, 1987). $\boldsymbol{t}$ must take equal and opposite values at two corresponding points of the boundary of the RVE, ∂V, that is, $\boldsymbol{t}$ must be anti-periodic on ∂V. $\boldsymbol{u}$ must be of the form:

$$\boldsymbol{u}(\boldsymbol{x}) = \boldsymbol{u}_0 + (\boldsymbol{E} + \boldsymbol{\Omega})\boldsymbol{x} + \tilde{\boldsymbol{u}}(\boldsymbol{x}), \tag{2}$$

with $\tilde{\boldsymbol{u}}$ periodic over V; $\boldsymbol{u}_0$ and the anti-symmetric second-order tensor $\boldsymbol{\Omega}$ define any (infinitesimal) rigid-body motion of the RVE. A displacement field fulfilling Eq. (2) is also said to be 'strain-periodic' (Suquet, 1987). No macroscopic strain is associated with $\tilde{\boldsymbol{u}}$. For periodic media, the appropriateness of $\boldsymbol{\Sigma}$ and $\boldsymbol{E}$ as mechanically meaningful macroscopic variables is supported by the rate-of-work equivalence (also known as 'Hill's macro-homogeneity equality'):

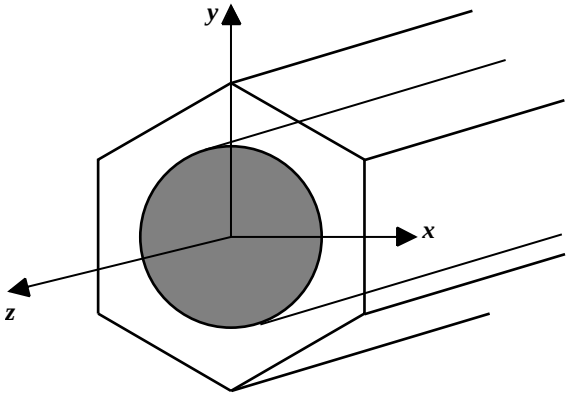

Fig. 1. RVE for a composite reinforced by a periodic hexagonal array of long, parallel fibers.

$$\boldsymbol{\Sigma} : \dot{\boldsymbol{E}} = \frac{1}{|V|} \int_V \boldsymbol{\sigma} : \dot{\boldsymbol{\epsilon}} \, \mathrm{d}V, \tag{3}$$

which shows that, for periodic media, $\boldsymbol{\Sigma}$ and $\dot{\boldsymbol{E}}$ are conjugate variables in the expression of the rate-of-work referred to any unit cell. Eq. (3) is the basis of energy approaches to evaluate bounds to the yield strength of fiber composites (Suquet, 1982; de Buhan and Taliercio, 1991; Taliercio, 1992; Taliercio and Sagramoso, 1995).

The incremental macroscopic (or homogenized) constitutive law of any composite with periodic structure can obtained, for instance, by imposing a given macroscopic stress increment to the unit cell and finding the corresponding macroscopic strain rate. This amounts at solving the following problem for the unit cell:

Given $\dot{\boldsymbol{\Sigma}}$, find $\dot{\boldsymbol{E}}(\dot{\boldsymbol{u}})$ such that

$$\dot{\boldsymbol{\Sigma}} = \frac{1}{|V|} \int_V \dot{\boldsymbol{\sigma}}(\boldsymbol{x}) \, \mathrm{d}V \tag{4}$$

$$\operatorname{div} \dot{\boldsymbol{\sigma}} = \boldsymbol{0} \quad \text{in } V \tag{5}$$

$$\dot{\boldsymbol{t}} = \dot{\boldsymbol{\sigma}} \boldsymbol{n} \quad \text{anti-periodic on } \partial V \tag{6}$$

$$\dot{\boldsymbol{E}} = \frac{1}{|V|} \int_V \dot{\boldsymbol{\epsilon}}(\boldsymbol{x}) \, \mathrm{d}V \tag{7}$$

$$\dot{\boldsymbol{u}} - \dot{\boldsymbol{E}} \boldsymbol{x} \quad \text{periodic on } V \tag{8}$$

$$\dot{\boldsymbol{\sigma}} = f(\dot{\boldsymbol{\epsilon}}(\dot{\boldsymbol{u}})) \quad \text{in } V. \tag{9}$$

Eq. (9) is symbolically the microscopic constitutive law in rate form at any point of the RVE.

The problem (4)–(9) is well posed, for instance, in the linear elastic case or when dissipative standard components are dealt with (Suquet, 1982).

3. The proposed finite element model

3.1. 2-D finite elements with 3-D strains invariant along an axis

The appropriate kinematic assumption for the analysis of any RVE of a composite reinforced by an array of long, parallel fibers is that the RVE is in a state of *generalized plane strain* (GPS), that is, the strain field is invariant along the fiber axis, z, owing to the assumed infinite length of the fiber: $\boldsymbol{\epsilon} = \boldsymbol{\epsilon}(x, y)$. Thus, the displacement field must be, at most, linear in z; in particular, the axial strain ϵ_z is necessarily constant throughout the RVE.

In order to match this kinematic requirement, a 'slice' of any 3-D RVE can be analyzed through conventional finite elements, with suitable boundary conditions. This was done, e.g., by Aghdam et al. (2001), Xia et al. (2003), Brockenbrough et al. (1991), and Carvelli and Taliercio (1999b). In the latter two works the macroscopic properties of elastic–plastic FRCs are estimated by discretizing the RVE with 8-noded isoparametric 'brick' elements, which allow the displacement field to vary linearly along any direction (provided that the elements are undistorted). Fig. 2 shows the 3-D finite element mesh employed by Carvelli and Taliercio (1999b): during deformation, the faces of the mesh orthogonal to the fiber axis were kept parallel, so as to enforce GPS conditions throughout the volume.

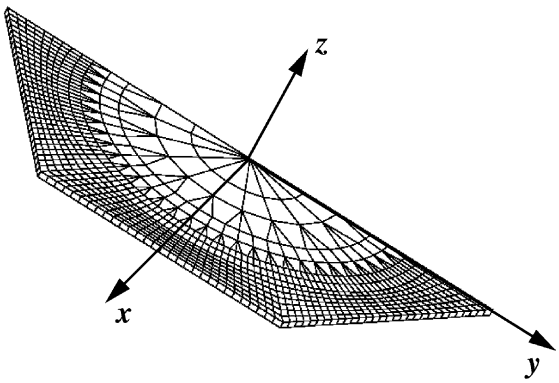

Fig. 2. Discretization of the RVE with 3-D finite elements.

A computationally expedient alternative to 3-D elements consists in formulating 2-D finite elements endowed with the kinematics of a continuum in GPS conditions. This was proposed by Taliercio and Carvelli (1999), who developed plane finite elements capable of describing a 3-D strain field invariant along the fiber axis to estimate the macroscopic elastic properties of FRCs through the analysis of the cross-section of any RVE. The kinematics of these elements is briefly recalled here. From here onwards, a matrix notation will be employed, unless explicit notice.

Consider a finite element (e) with $n^{(e)}$ nodes; each node has three degrees of freedom, corresponding to the components of the nodal displacement $\boldsymbol{U}_j^{(e)} = \{u_j^{(e)}, v_j^{(e)}, w_j^{(e)}\}^{\mathrm{T}}, j = 1 \ldots n^{(e)}$. Each component of the displacement field, $\boldsymbol{u}(\boldsymbol{x}) = \{u(\boldsymbol{x}), v(\boldsymbol{x}), w(\boldsymbol{x})\}^{\mathrm{T}}$, is modeled so as to depend linearly on z over any element; concisely:

$$\boldsymbol{u}^{(e)}(x, y, z) = \boldsymbol{N}^{(e)}(x, y)\boldsymbol{U}^{(e)} + z\boldsymbol{E}_z, \tag{10}$$

where $\boldsymbol{U}^{(e)}$ collects the $3 \times n^{(e)}$ nodal degrees of freedom and $\boldsymbol{E}_z = \{2E_{zx}, 2E_{zy}, E_{zz}\}^{\mathrm{T}}$ is an array gathering three additional degrees of freedom (d.o.fs), common to all the elements into which the RVE has been discretized; E_{zx}, E_{zy} and E_{zz} can be interpreted as three of the macroscopic strain components, once the periodicity of the strain field has been enforced. If the proposed finite elements have to be implemented in a finite element code with user-oriented interface, it can be computationally expedient to associate these additional d.o.fs with a fictitious node ('node 0'), shared by all the elements forming the mesh. Assembly is then performed in the usual way, accounting for the fictitious node in the connection table. Fig. 3 schematically shows finite elements with three or four nodes of the type proposed in this work.

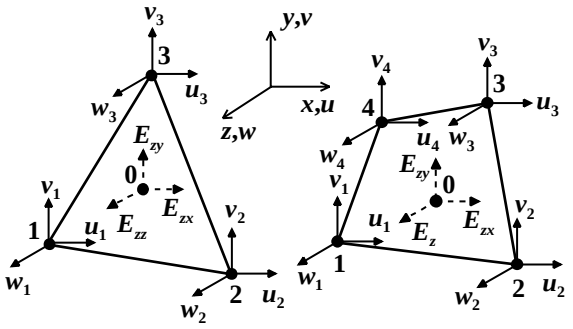

Fig. 3. Three- and four-noded 2-D elements with out-of-plane linear modeling of the displacements.

Alternatively, only the periodic term in the microscopic displacement field, Eq. (2), might be modeled through shape functions (Débordes, 1986): in this case, all of the six macroscopic strain components can be interpreted as d.o.fs shared by all of the elements.

From here onwards the superscript (e) defining any element will be omitted for the sake of brevity. $\boldsymbol{N}$ is the in-plane shape matrix, which modelizes the displacement field in the plane (x,y) orthogonal to the fiber axis. As usual, $\boldsymbol{N}$ can be split into 3×3 sub-matrices, each one pertinent to one of the nodes:

$$\boldsymbol{N}_j(x,y) = N_j(x,y)\begin{bmatrix}1 & 0 & 0\\ 0 & 1 & 0\\ 0 & 0 & 1\end{bmatrix}, \quad j = 1\ldots n; \tag{11}$$

here, the same type of discretization has been employed for all three of the displacement components.

Let $\boldsymbol{\epsilon} = \{\epsilon_x, \epsilon_y, \epsilon_z, \gamma_{xy}, \gamma_{zx}, \gamma_{zy}\}^{\mathrm{T}}$ be the array gathering the six independent (infinitesimal) engineering strains (i.e., axial and shearing strains). The strain field associated with Eq. (10) over any element has the form

$$\boldsymbol{\epsilon}(x,y) = \boldsymbol{B}_U(x,y)\boldsymbol{U} + \boldsymbol{B}_E\boldsymbol{E}_z. \tag{12}$$

$\boldsymbol{B}_E$ is the constant matrix

$$\boldsymbol{B}_E = \begin{bmatrix}0 & 0 & 0\\ 0 & 0 & 0\\ 0 & 0 & 1\\ 0 & 0 & 0\\ 1 & 0 & 0\\ 0 & 1 & 0\end{bmatrix}; \tag{13}$$

$\boldsymbol{B}_U$ is the in-plane compatibility matrix, which can be split into 6×3 sub-matrices $\boldsymbol{B}_{Uj}$, $j = 1\ldots n$, each one defining the contribution of the j-th nodal displacement to the in-plane modeling of the strain field. Each sub-matrix is given by

$$\boldsymbol{B}_{Uj} = \begin{bmatrix}\frac{\partial N_j}{\partial x} & 0 & 0\\ 0 & \frac{\partial N_j}{\partial y} & 0\\ 0 & 0 & 0\\ \frac{\partial N_j}{\partial y} & \frac{\partial N_j}{\partial x} & 0\\ 0 & 0 & \frac{\partial N_j}{\partial x}\\ 0 & 0 & \frac{\partial N_j}{\partial y}\end{bmatrix}, \quad j = 1\ldots n. \tag{14}$$

Considering an element made of elastic–plastic material, the (tangent) stiffness matrix, $\boldsymbol{K}$, can be expressed as

$$\boldsymbol{K} = \begin{bmatrix}\boldsymbol{K}_{UU} & \boldsymbol{K}_{UE}\\ \boldsymbol{K}_{UE}^{\mathrm{T}} & \boldsymbol{K}_{EE}\end{bmatrix}, \tag{15}$$

where, denoting by A the domain occupied by any finite element in the plane (x,y):

$$\boldsymbol{K}_{UU} = \int_A \boldsymbol{B}_U^{\mathrm{T}}(x,y)\boldsymbol{D}(x,y)\boldsymbol{B}_U(x,y)\,\mathrm{d}x\,\mathrm{d}y, \tag{16}$$

$$\boldsymbol{K}_{UE} = \left(\int_A \boldsymbol{B}_U^{\mathrm{T}}(x,y)\boldsymbol{D}(x,y)\,\mathrm{d}x\,\mathrm{d}y\right)\boldsymbol{B}_E, \tag{17}$$

$$\boldsymbol{K}_{EE} = \boldsymbol{B}_E^{\mathrm{T}}\left(\int_A \boldsymbol{D}(x,y)\,\mathrm{d}x\,\mathrm{d}y\right)\boldsymbol{B}_E. \tag{18}$$

$\boldsymbol{D}$ is the 6×6 matrix defining the incremental stress–strain law for an elastic–plastic material: $\dot{\boldsymbol{\sigma}} = \boldsymbol{D}\dot{\boldsymbol{\epsilon}}$. If the stress point lies inside the elastic domain, or the stress point is at yielding but the stress increment points 'inwards' the current elastic domain, $\boldsymbol{D}$ is the elastic matrix, $\boldsymbol{D}^{\mathrm{el}}$. If the stress point is at yielding, and the stress increment keeps it on the current yield surface, $\boldsymbol{D}$ is the elastic–plastic matrix. In standard plasticity, $\boldsymbol{D}$ is given by (see e.g. Owen and Hinton, 1980):

$$\boldsymbol{D} = \boldsymbol{D}^{\mathrm{el}}\left(\boldsymbol{I} - \frac{\boldsymbol{n}\boldsymbol{n}^{\mathrm{T}}\boldsymbol{D}^{\mathrm{el}}}{h + \boldsymbol{n}^{\mathrm{T}}\boldsymbol{D}^{\mathrm{el}}\boldsymbol{n}}\right), \tag{19}$$

where $\boldsymbol{I}$ is the identity matrix, $\boldsymbol{n}$ is the unit vector outward normal to the elastic domain at the current stress point, and h is a hardening parameter.

For finite elements made of linearly elastic, homogeneous, isotropic materials, the explicit expressions for the matrices $\boldsymbol{K}_{UE}$ and $\boldsymbol{K}_{EE}$ can be found in Taliercio and Carvelli (1999).

The discretization of any RVE presented in Section 3.2 makes use of finite elements with three or four nodes each (see Fig. 3). The four-noded element is obtained by mapping the classical square 'parent' element onto the (x,y) plane with the same shape functions that model the displacement field. Thus, the employed elements behave similarly to classical CST and ISOP4 2-D elements as far as the modelization of the displacement field on the in-plane coordinates is concerned. Note, however, that the proposed elements cannot be strictly regarded as isoparametric, because of the presence of the axial coordinate z in the modelization of the displacement field.

3.2. Boundary conditions for the discretized RVE

The discretization made to analyze a typical RVE of a periodically reinforced fiber composite is analogous to that employed by Taliercio and Coruzzi (1999) to predict the macroscopic response of linearly elastic and brittle-matrix composites under plane strain conditions. Owing to symmetry considerations, only half of the RVE can be discretized. Fig. 4 shows the finite element mesh used in the applications: it consists of 890 four-noded elements and 90 three-noded elements. The total number of nodes, each one having three d.o.fs, is 1114; the fictitious node with $\boldsymbol{E}_z$ as d.o.fs completes the mesh. In Fig. 4 the mid-points of the four sides of the mesh are denoted by J, H, K, and O.

The kinematic conditions to be imposed at the boundary of the discretized RVE to match the periodicity of $\tilde{\boldsymbol{u}} = \tilde{\boldsymbol{u}}(x,y)$ in Eq. (2), and amount to

$$\boldsymbol{u}_C = \frac{\boldsymbol{u}_A + \boldsymbol{u}_B}{2}, \tag{20}$$

where $\boldsymbol{u}_P$ is the displacement at any point P. Here, (A,B) is any pair of nodes on any side of the RVE, symmetric with respect to the mid-point (C) of that side (with $C = J$, H, K or O). A condition has to be added to ensure the compatibility of the deformed sides of the mesh, namely

$$\boldsymbol{u}_O + \boldsymbol{u}_H = \boldsymbol{u}_J + \boldsymbol{u}_K. \tag{21}$$

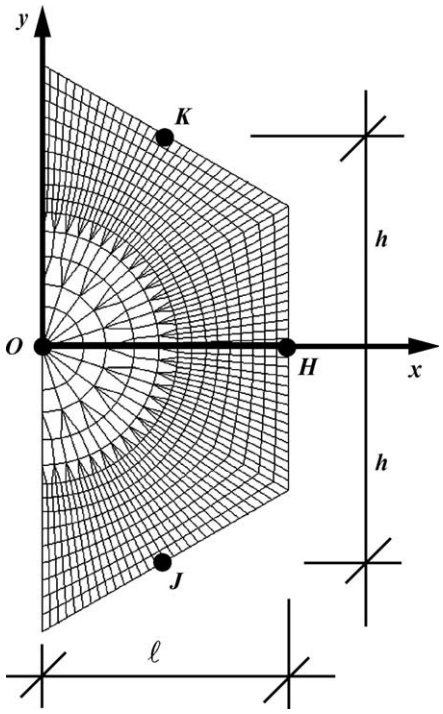

Fig. 4. Discretization of the RVE with 2-D finite elements.

Further details on these conditions can be found in Taliercio and Coruzzi (1999). Eqs. (20) and (21) involve the total boundary displacements and are easier to implement in existing finite element codes than conditions dealing with the periodic term $\tilde{\boldsymbol{u}}(x,y)$ (see e.g. Francescato and Pastor, 1997). An alternative form of the boundary conditions was employed by Xia et al. (2003), who imposed that any two opposite sides of the deformed RVE remain parallel, thus meeting both the requirements of strain periodicity and displacement continuity across adjacent RVEs. As shown in Taliercio and Coruzzi (1999), the two forms of boundary conditions are actually coincident.

Finally, consider the conditions preventing any rigid body motion of the RVE. Rigid translations can be suppressed, e.g., by setting $\boldsymbol{u}_O = \boldsymbol{0}$. Since periodicity requires $\tilde{\boldsymbol{u}}_C = \boldsymbol{0}$ at the mid-points of any side of the mesh, application of Eq. (2) at H and K yields (see Fig. 4):

$$u_H = E_{xx}\ell, \quad v_H = (E_{yx} + \Omega_{yx})\ell, \quad w_H = (E_{zx} + \Omega_{zx})\ell; \tag{22}$$

$$u_K = E_{xx}\frac{\ell}{2} + (E_{xy} + \Omega_{xy})h, \quad v_K = (E_{yx} + \Omega_{yx})\frac{\ell}{2} + E_{yy}h, \quad w_K = (E_{zx} + \Omega_{zx})\frac{\ell}{2} + (E_{zy} + \Omega_{zy})h. \tag{23}$$

Accounting for Eqs. (22) and (23), the condition $\boldsymbol{\Omega} = \boldsymbol{0}$ which suppresses any (infinitesimal) rigid rotation of the RVE implies:

$$\frac{v_H}{\ell} = \frac{u_K - u_H/2}{h}, \quad E_{zx} = \frac{w_H}{\ell}, \quad E_{zy} = \frac{w_K - w_H/2}{h}. \tag{24}$$

Also, Eqs. (22) and (23) allow one to relate the in-plane displacements of nodes H and K with three of the other macroscopic strains:

$$E_{xx} = \frac{u_H}{\ell}, \quad E_{yy} = \frac{v_K - v_H/2}{h}, \quad E_{xy} = \frac{v_H}{\ell}. \tag{25}$$

Eqs. (24) and (25) can be directly exploited to analyze the RVE under any macroscopic strain, by simply prescribing the values of some d.o.fs (and/or relations between them). These d.o.fs, namely u_H, v_H,v_K, E_{zx}, E_{zy}, and E_{zz}, will be called 'master degrees of freedom' in the continuation of this paper.

Owing to symmetry considerations, it is also possible to model elementary macroscopic stresses by giving some of the d.o.fs prescribed values. Table 1 summarizes which d.o.fs have to be prescribed to reproduce any elementary macroscopic stress in the RVE; the remaining 'master' d.o.fs are implicitly free. It goes without saying that, beyond the linear elastic range, non-elementary stresses (e.g., off-axis tension, biaxial tension, etc.) cannot be reproduced by simply prescribing any d.o.f.

Recently, Jiang et al. (2002) discussed the influence of the boundary conditions on the predicted macroscopic elastic and elastoplastic response of periodic 2D composites. They concluded that, as far as the loading conditions considered in their work are concerned, the response predicted using periodic boundary conditions is the same as that predicted using special 'mixed' boundary conditions, involving both boundary tractions and displacements. If uniform boundary displacements, or uniform boundary tractions, are prescribed, bounds on the response predicted using periodicity conditions are obtained. The gap between the bounds narrows as the mismatch in properties between the phases decreases, and as the size of the RVE (consisting of several unit cells) increases.

3.3. Modified compliance matrix for incompressible deformations

It is well known that finite element solutions dealing with incompressible materials are prone to 'locking' effects when approaching the fully plastic range. Several techniques have been proposed to circumvent this problem, such as the selected integration of the tangent stiffness matrix, with a reduced integration of the volumetric term (Malkus and Hughes, 1978). Another possibility is the use of 'enhanced strain'-based elements: this was done, e.g., by Capsoni and Corradi (1997) to predict the ultimate carrying capacity of structures in plane strain conditions, and later applied by Carvelli and Taliercio (1999a) to compute the macroscopic strength of FRCs under transversal stresses.

The approach proposed by Nagtegaal et al. (1974) is very effective for practical applications: it is based on the definition of a modified functional, depending only on kinematic variables, whose stationarity conditions imply the incompressibility constraint to be approximately fulfilled over any element. In the case of 4-noded quadrilateral elements, it was shown by the authors that, enforcing incompressibility in an average (or 'weak') form, actually makes the functional to depend on a 'modified strain rate tensor', defined as

$$\dot{\boldsymbol{\epsilon}}^* = \frac{1}{2}(\nabla \dot{\boldsymbol{u}} + (\nabla \dot{\boldsymbol{u}})^{\mathrm{T}}) + \frac{1}{3}(\langle \mathrm{div} \dot{\boldsymbol{u}} \rangle - \mathrm{div} \dot{\boldsymbol{u}}) \boldsymbol{I} \tag{26}$$

Table 1
Correspondence between 'master' degrees of freedom of the model and simulated macroscopic stress

Macrostress component	Prescribed d.o.fs
Σ_{xx}	u_H
Σ_{yy}	v_K ($u_H = 0$)
Σ_{zz}	E_{zz}
Σ_{xy}	v_H
Σ_{zx}	E_{zx}
Σ_{zy}	E_{zy}

where $\langle \cdot \rangle$ denotes volume average over any finite element and $\boldsymbol{I}$ is the identity tensor. Note that only the direct strain components are modified, whereas $\gamma^*_{xy} = \gamma_{xy}$, $\gamma^*_{zx} = \gamma_{zx}$, $\gamma^*_{zy} = \gamma_{zy}$. More complicated definitions are required for higher-order elements. The main advantage is that this approach can be easily implemented in existing finite element codes, as one needs only to re-define the compatibility matrix converting nodal displacements into strains. Incidentally note that this is the technique implemented in the commercial finite element code ABAQUS© to prevent locking in first-order elements (see ABAQUS Theory Manual, ver. 5.7, 1997).

Only 4-noded quadrilateral elements will be dealt with in this section. The compatibility matrix of the 3-noded elements in the mesh discretizing the RVE in Fig. 4 needs no modifications respect to that presented in Section 3, since the incompressibility constraint does not induce significant locking effects in these elements (Nagtegaal et al., 1974). Accounting for the modified definition of the strain rates, the array gathering the modified strain components can be expressed as

$$\boldsymbol{\epsilon}^* = \boldsymbol{B}^*_U \boldsymbol{U} + \boldsymbol{B}_E \boldsymbol{E}_z \tag{27}$$

where only the submatrix $\boldsymbol{B}^*_U$ has to be modified respect to Eq. (12). If $\boldsymbol{B}^*_U$ is split into four 6×3 submatrices, similarly to Section 3.1, Eq. (14) has to be replaced by:

$$\boldsymbol{B}^*_{Uj} = \begin{bmatrix} \frac{1}{3}\left(2\frac{\partial N_j}{\partial x} + \left\langle \frac{\partial N_j}{\partial x} \right\rangle\right) & -\frac{1}{3}\left(\frac{\partial N_j}{\partial y} - \left\langle \frac{\partial N_j}{\partial y} \right\rangle\right) & 0 \\ -\frac{1}{3}\left(\frac{\partial N_j}{\partial x} - \left\langle \frac{\partial N_j}{\partial x} \right\rangle\right) & \frac{1}{3}\left(2\frac{\partial N_j}{\partial y} + \left\langle \frac{\partial N_j}{\partial y} \right\rangle\right) & 0 \\ -\frac{1}{3}\left(\frac{\partial N_j}{\partial x} - \left\langle \frac{\partial N_j}{\partial x} \right\rangle\right) & -\frac{1}{3}\left(\frac{\partial N_j}{\partial y} - \left\langle \frac{\partial N_j}{\partial y} \right\rangle\right) & 0 \\ \frac{\partial N_j}{\partial y} & \frac{\partial N_j}{\partial x} & 0 \\ 0 & 0 & \frac{\partial N_j}{\partial x} \\ 0 & 0 & \frac{\partial N_j}{\partial y} \end{bmatrix}, \quad j = 1 \ldots 4. \tag{28}$$

Fig. 5 illustrates the positive effects of this modifications when the FE model shown in Fig. 4 is submitted to uniaxial transverse tension. Both phases of the composite are assumed to be elastic–perfectly plastic. If the

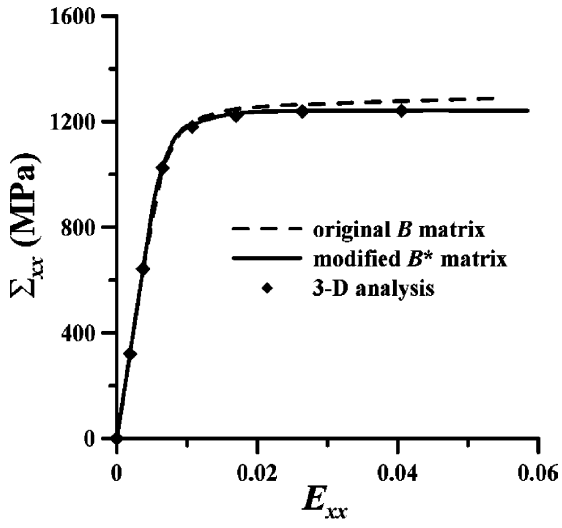

Fig. 5. Simulation of a tension test transverse to the fibers with the proposed model: finite element results with a conventional compatibility matrix and a matrix modified according to Nagtegaal et al. (1974). The results obtained with ABAQUS© and the 3-D mesh in Fig. 2 are also shown.

traditional compatibility matrix ($\boldsymbol{B}_U$) is employed for the 4-noded elements, no macroscopic yield stress is detected, and the FE model exhibits a fictitiously hardening response (dashed line). If the compatibility matrix is changed into $\boldsymbol{B}_U^*$ according to the procedure outlined above, the correct perfectly plastic macroscopic response can be captured (solid line). For the sake of comparison, in Fig. 5 the results are plotted of FE analyses performed with ABAQUS© on the 3-D model shown in Fig. 2, with boundary constraints enforcing both in-plane periodicity of the strain field and GPS conditions. The results of this analysis are perfectly superposed to those of the 2-D model with modified compatibility matrix. It is worth emphasizing that a fully 3-D analysis is computationally much more cumbersome than the proposed model, as it involves nearly three times the number of kinematic constraints of the 2-D model.

4. Numerical applications

Unless otherwise stated, the numerical applications described in these section refer to Ti/SCS, with titanium 6Al–4V matrix and fibers in silicon carbide. The fiber volume fraction (v_f) is 0.40. The elastic constants (E, v) and the yield stress (σ_0) of the components are reported in Table 2. Some comparisons with the results of tests on B–Al specimens are also reported in Section 4.2. Both components are supposed to comply with J_2'-plasticity.

4.1. Predicting the non-linear response to failure of metal–matrix composites

The finite element model shown in Fig. 4 was first analyzed under elementary macroscopic stress histories. In these analyses, one of the 'master' d.o.fs is progressively increased by letting the other ones free, so as to have only one non-vanishing macroscopic stress per time, according to Table 1. The analyses end up as a numerical 'macroscopic yielding' is detected, that is, the value of the macroscopic stress does not significantly change from one load step to another. The results of these analyses are presented in Fig. 6 in the form of contour plots of the equivalent plastic strain at the 'macroscopic yielding', which is matched by the formation of shear bands in the RVE. If a macroscopic axial stress Σ_{zz} is applied, strains are uniform throughout the fiber and the matrix: this case is not shown in Fig. 6.

The discretized RVE was also subjected to a number of radial loading paths in the space of the macroscopic strains: the d.o.fs corresponding to the macroscopic strain components E_{xx}, E_{yy} and E_{zz} (see Eqs. (24) and (25)) were monotonically increased by keeping their ratios equal to prescribed constant values. The remaining 'master' d.o.fs are free. Accordingly, the stress point in the space of the macroscopic stresses moves along paths which are radial when the stress at any point in the RVE lies within the local elastic domain, but which deviate from linearity when plasticity develops within the RVE. Owing to symmetry considerations, the macroscopic stress associated with the prescribed macroscopic strain has zero cartesian shear components: thus, Σ_{xx}, Σ_{yy} and Σ_{zz} are macroscopic principal stresses.

Figs. 7 and 8 show the stress points along the different loading paths considered: Fig. 7 refers to loading paths with E_{zz} free (so that $\Sigma_{zz} = 0$); in Fig. 8 the stress points along any loading path are projected onto the

Table 2
Elastic properties and yield stress for matrix and fiber of Ti/SCS (after Sun et al., 1990)

	E (GPa)	v	σ_0 (MPa)
Matrix (Ti-6-4)	109	0.34	980
Fiber (SCS-6)	427.6	0.25	3000

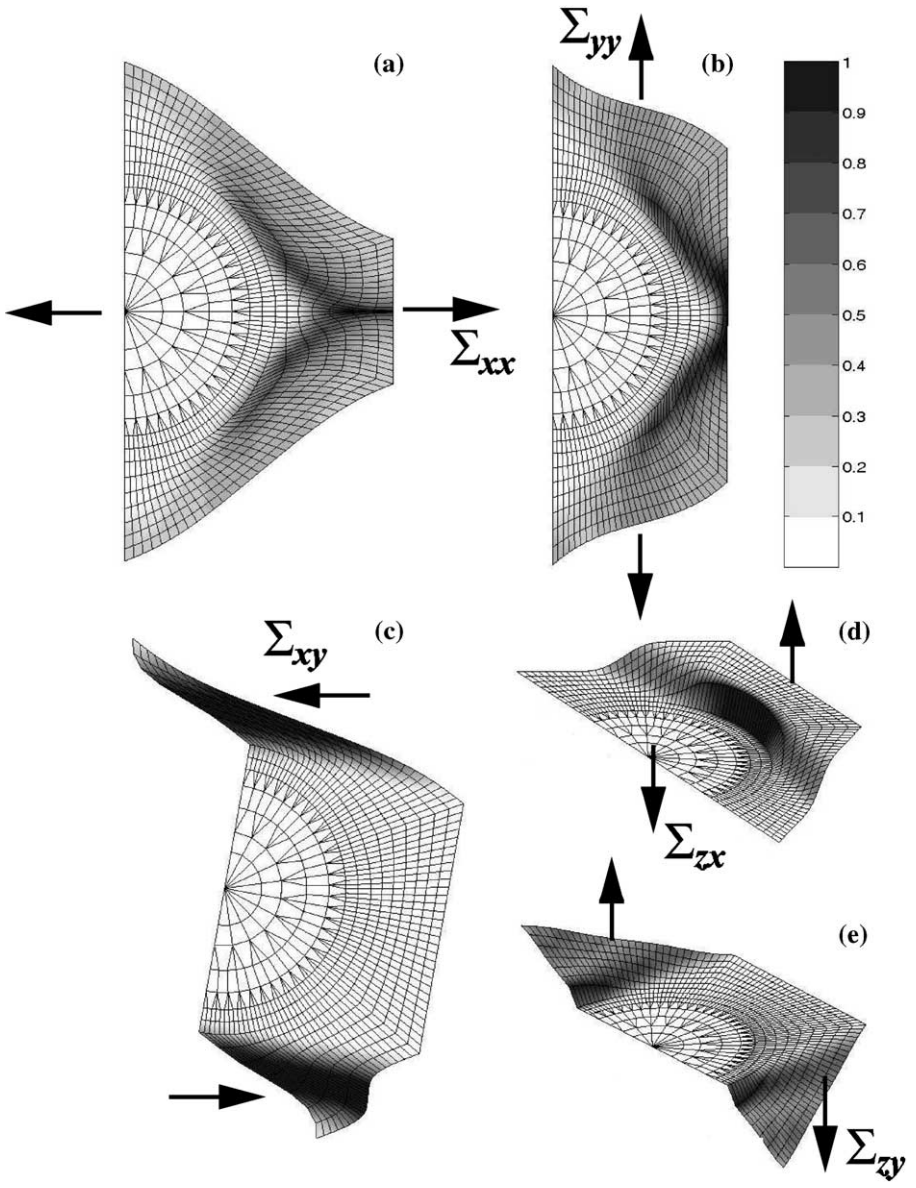

Fig. 6. Contour plots of the equivalent plastic strain at the macroscopic yielding in numerical tests with one macroscopic stress applied to the RVE: (a) Σ_{xx}; (b) Σ_{yy}; (c) Σ_{xy}; (d) Σ_{zx}; (e) Σ_{zy}.

deviatoric plane Π. The envelope of these loading paths (which is not explicitly drawn in these figures, to avoid confusion) is the numerically detected macroscopic yield locus for the composite.

It is interesting to compare the 'macroscopic strength domain', G^{hom}, obtained through the finite element model presented and some theoretical approximations of this domain available in the literature. G^{hom} is defined as the set of macroscopic stresses associated with periodic, statically and plastically admissible microscopic stress fields within the RVE (Suquet, 1982). The theoretical bases for the definition of bounds to G^{hom} are briefly recalled in the Appendix. The sections of these bounds for Ti/SCS are shown in Figs. 7

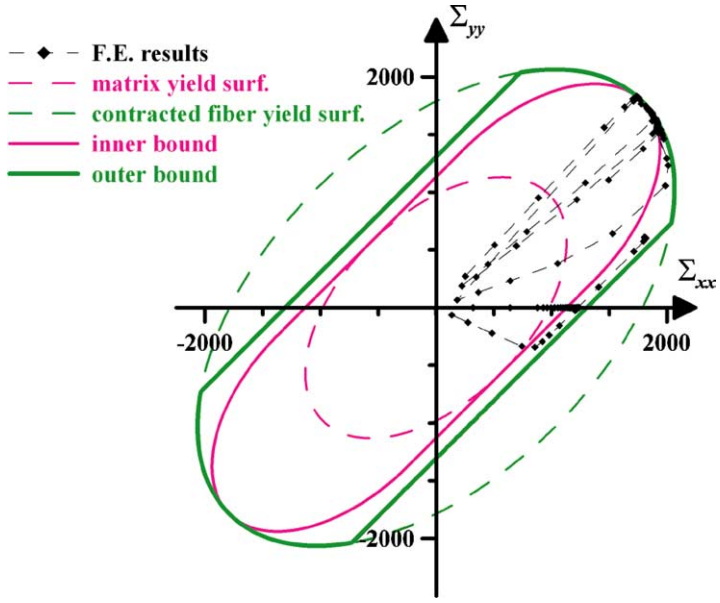

Fig. 7. RVE subjected to biaxial principal stresses aligned with x and y: numerically identified yield locus and theoretical bounds for the macroscopic strength domain in the plane (Σ_{xx}, Σ_{yy}).

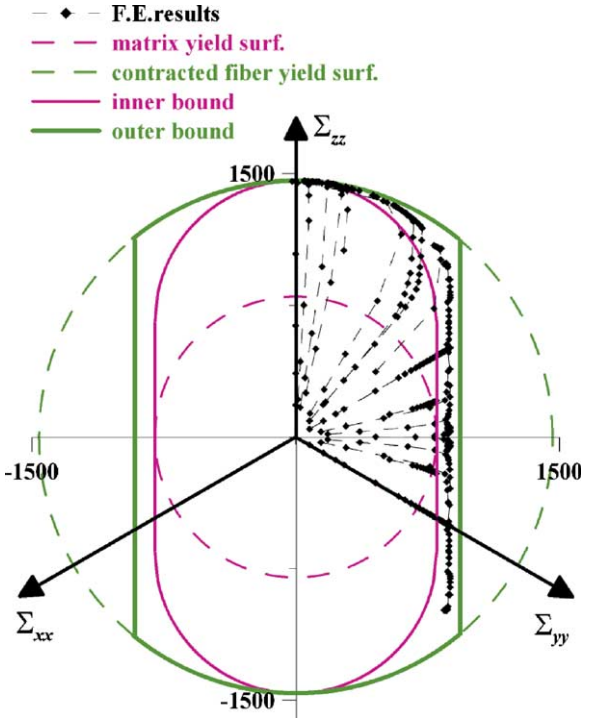

Fig. 8. RVE subjected to triaxial principal stresses aligned with x, y and z: numerically identified yield locus and theoretical bounds for the macroscopic strength domain in the deviatoric plane Π.

and 8 (solid lines) and compared with the sections of the numerically identified macroscopic yield locus in the corresponding planes. For the sake of comparison, in these figures the yield domain of the unreinforced matrix and the yield domain of the fiber material, homothetically contracted as discussed in the Appendix, are also shown. The theoretical bounds are perfectly consistent with the numerical findings of the present work: all the macroscopic stress paths end in the region comprised between the inner and outer bounds to the macroscopic yield surface.

4.2. Comparisons with experimental results

Table 3 summarizes the macroscopic elastic constants for Ti/SCS identified through the present numerical model, by submitting the discretized RVE to elementary stresses. These values are compared with the experimental ones reported by Sun et al. (1990) and the elastic coefficients estimated according to Mori–Tanaka theory (Benveniste, 1987). Note that the axial shear modulus, G_{zx}, was not directly measured by the experimenters, but simply estimated in order to best fit some experimental curves. On account of the scatter in the test data documented by the experimenters, the comparison is satisfactory on the whole.

The capabilities of the proposed model in predicting the macroscopic strength properties of elastic–plastic composites were assessed through comparisons with results available in the literature. Since the possibility of failure at the fiber–matrix interface is not allowed for in the present version of the model, comparisons can only be made with the results of tests on 'strongly-bonded composites'. Tests made on 'weakly-bonded composites' could be considered provided that the failure mode of the composite does not involve the interface (e.g., tension tests nearly collinear with the fibers).

According to these requirements, the results of Dvorak et al. (1988) were selected. These authors determined the initial yield surface and the subsequent yield surfaces of B–Al composites subjected to several multiaxial loading programs. The tests were carried out on axially reinforced tubular specimens, which were tested under combined axial force, torque and internal pressure. Only comparisons with the experimentally detected initial yield surface are possible with the present version of the proposed model, which does not allow for hardening. No mention is made by the experimenters of debonding phenomena at the fiber–matrix interface. The fiber volume fraction $v_f = 0.45$. The uniaxial yield strength of the components is $\sigma_{0m} = 17.9\,\text{MPa}$ for aluminium and $\sigma_{0f} = 168\,\text{MPa}$ for boron.

Fig. 9 illustrates to the results of tests with combined longitudinal tension and longitudinal shear, whereas Fig. 10 refers to tests with combined transverse tension and longitudinal shear. In both figures, the test data are plotted together with the macroscopic stress points obtained by the finite element analyses and the theoretical bounds to the macroscopic yield surface computed according to the procedure recalled in the Appendix. The strength data are normalized to the uniaxial strength of the unreinforced matrix, $\tau_0 = \sigma_{0m}/\sqrt{3}$. Each of the numerical analyses referred to in Fig. 9 (resp., in Fig. 10) was carried out by prescribing the ratio of the d.o.fs v_H/E_{zz} (resp., v_H/E_{zx}) to take different selected values. The remaining 'master' d.o.fs are free. The theoretical predictions match the test data with a good accuracy.

Table 3
Macroscopic elastic constants for Ti/SCS: experimental data, FE estimates, and predictions using Mori–Tanaka theory

	Test data (after Sun et al., 1990)	Numerical model (% diff.)	Mori–Tanaka method
E_x, E_y (GPa)	150.3	175.9 (+17.0)	175.9
E_z (GPa)	230.3	236.6 (+2.7)	236.7
G_{xy} (GPa)	–	65.09	64.43
G_{zx}, G_{zy} (GPa)	62.1[a]	67.63 (+8.9)	67.26
v_{xy}	–	0.3511	0.3653
v_{zx}, v_{zy}	0.25	0.2189 (–12.4)	0.2233

[a] Indirect estimate.

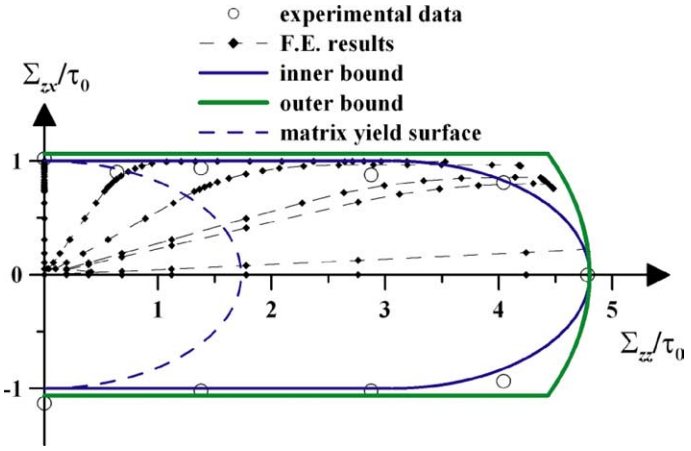

Fig. 9. Initial yield surface of B–Al under combined axial tension and shear: comparison of experimental data (after Dvorak et al., 1988), numerically identified yield locus and theoretical bounds for the macroscopic strength domain.

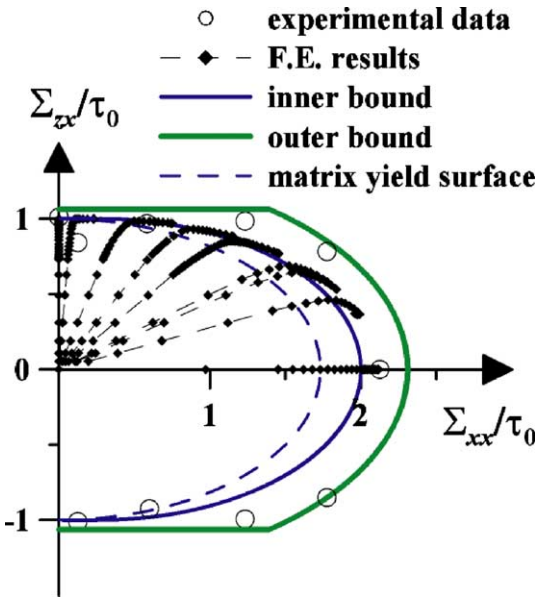

Fig. 10. Initial yield surface of B–Al under combined transverse tension and axial shear: comparison of experimental data (after Dvorak et al., 1988), numerically identified yield locus and theoretical bounds for the macroscopic strength domain.

5. Concluding remarks and future perspectives

A numerical model was developed to predict the non-linear macroscopic mechanical response to failure of elastic–plastic composites, reinforced by a regular array of continuous, parallel fibers, under any loading condition (in terms of macroscopic stresses or strains).

The model consists of a mesh of plane finite elements, which discretizes any cross-section of a representative volume element. An original characteristic of the model is that the finite elements proposed in this

paper are capable of describing particular three-dimensional strain fields, invariant along the fiber axis. The compatibility matrix of the elements was modified according to the proposal of other authors, to prevent 'locking' effects in the plastic range. Suitable periodicity boundary conditions are enforced along the sides of the RVE to conform to the regularity of the reinforcing array.

The model was implemented into a commercial, non-linear finite element code (ABAQUS) endowed with a user-oriented interface, capable of dealing with multi-point kinematic constraints. Several analyses were carried out, which showed that the numerical results perfectly match previously obtained analytical predictions for the macroscopic strength domain of FRCs and agree with available experimental data fairly well.

The model turns out to be definitely superior in terms of computational effort to fully 3-D models and allows one to predict the response of FRCs under loading conditions that 'standard' 2-D models could not reproduce.

Future developments of the model will include the possibility of allowing for debonding at the fiber–matrix interface, a mode of failure which is quite common under stresses such as transverse tension for weakly bonded composites. Also, the model could be extended to FRCs with strainhardening components, as briefly outlined in Section 3.1.

Acknowledgments

The assistance of Mr. Valerio Lunati in software developing and data processing is gratefully acknowledged. The author also wishes to thank Dr. Valter Carvelli, for placing the original software at his disposal, and Dr. Giuseppe Cocchetti, for his most valuable assistance in the graphical output.

Appendix A. Definition of inner and outer bounds of the macroscopic strength domain of periodic composites

According to homogenization theory for periodic media applied to limit analysis (Suquet, 1987), an inner bound to the macroscopic strength domain, G^{hom}, of a composite reinforced by a regular array of fibers can be obtained by defining a suitable periodic, statically and plastically admissible microstress field within the RVE, which consists of a single elementary cell. A simple example of such field was proposed by de Buhan and Taliercio (1991) and, in tensor notation, reads

$$\boldsymbol{\sigma}(\boldsymbol{x}) = \boldsymbol{\sigma_m} + \chi(V_{\mathrm{f}})\sigma \boldsymbol{e}_z \otimes \boldsymbol{e}_z, \tag{A.1}$$

where χ is the indicator function of the part of RVE (V_{f}) occupied by the fiber, $\boldsymbol{e}_z$ is the unit vector of the fiber axis, $\boldsymbol{\sigma_m}$ is the (constant) stress in the matrix and σ is an additional uniaxial contribution to the stress in the fiber. Suppose that both the fiber and the matrix materials comply with J_2'-plasticity; let $r(\geqslant 1)$ be the ratio of the uniaxial fiber strength ($\sigma_{0\mathrm{f}}$) to the uniaxial matrix strength ($\sigma_{0\mathrm{m}}$). According to Eq. (A.1), an inner bound to G^{hom} in the space of the macroscopic stresses (simplified according to Taliercio, 1992) is

$$G_s = \{\boldsymbol{\Sigma} = \boldsymbol{\sigma_m} + v_{\mathrm{f}}\sigma \boldsymbol{e}_z \otimes \boldsymbol{e}_z, \quad \boldsymbol{\sigma_m} \in G_{\mathrm{m}}, \quad |\sigma| \leqslant \bar{\sigma}\} \quad (\subseteq G^{\mathrm{hom}}) \tag{A.2}$$

where G_{m} is the strength domain of the fiber material, $\bar{\sigma} = v_{\mathrm{f}}\sigma_{0\mathrm{m}}(r-1)$; $G_s = G_{\mathrm{m}}$ for a homogeneous RVE. This domain con be graphically constructed in the space of the macroscopic stresses by shifting G_{m} along the longitudinal stress axis, Σ_{zz}, of an amount equal to $\bar{\sigma}$ on the side of tensions and of an equal amount on the side of compressions: the convex envelope of the shifted domains is G_s (see, e.g., Figs. 8 and 9). This mechanically meaningful construction points out that, basically, the strengthening effect of the fibers affects the longitudinal strength of the composite, whereas the transverse and shear strengths of the FRC do not significantly differ from those of the unreinforced matrix.

An outer bound to $G^{\hom}$, G_k, can be obtained by computing the plastic power dissipated in any periodic 'failure mechanism' for the RVE, which, according to the kinematic theorem of limit analysis, is an upper bound to the actual dissipated macroscopic plastic power. The plastic power dissipated in any unit volume is proportional to the 'support function' (see e.g. Tyrrell-Rockafellar, 1970) of the material strength domain. Accordingly, in the case of von Mises-type constituents, G_k can be seen as the intersection of several domains in the space of the macroscopic stresses (Taliercio, 1992): a domain G_{f}^{*}, obtained by homothetically contracting the fiber strength domain of a coefficient $\rho = v_{\mathrm{f}} + (1-v_{\mathrm{f}})/r(\leqslant 1)$, which corresponds to uniform strain rate throughout the RVE (see Figs. 7 and 8, dashed lines), and three hypercylinders, all tangent to G_{m} and coaxial with the axis Σ_{zz}. The support functions of these hypercylinders correspond to the plastic power dissipated in failure mechanisms of the type schematically depicted in Fig. 11a and b, with rigid parts of the RVE relatively slipping one to each other along some failure planes. The unit normal to any one of these slip planes is denoted by $\boldsymbol{n}$: in Fig. 11a the slip planes have $\boldsymbol{n} = \boldsymbol{e}_y$, whereas $\boldsymbol{n} = \boldsymbol{n}_\beta$ for the slip planes in Fig. 11b. Similarly, mechanisms with slip planes orthogonal to $\boldsymbol{n} = \boldsymbol{e}_x$ can be constructed. Synthetically, the definition of any one of the three hypercylinders is:

$$G_{\mathrm{m}}^{*}(\boldsymbol{n}) = \left\{ \boldsymbol{\Sigma} : |T| \leqslant \frac{\sigma_{0\mathrm{m}}}{\sqrt{3}} \right\}, \tag{A.3}$$

where $|T|$ is the modulus of the macroscopic shear stress acting on the slip plane. Thus

$$G_k = G_{\mathrm{f}}^{*} \cap G_{\mathrm{m}}^{*}(\boldsymbol{e}_x) \cap G_{\mathrm{m}}^{*}(\boldsymbol{e}_y) \cap G_{\mathrm{m}}^{*}(\boldsymbol{n}_\beta). \tag{A.4}$$

If the fiber volume fraction is sufficiently high, the slip planes would have to cut the fiber, which is usually much stronger than the surrounding matrix: this might lead to excessively high upper bounds to the carrying capacity of the composite. Stricter upper bounds can be then obtained by considering mechanisms such as the one depicted in Fig. 11c, with a slip surface partially involving the fiber–matrix interface. This leads to upper bounds to the shear strength of the composite of the kind $|\Sigma_{zx}| \leqslant \rho_{\mathrm{f}}\sigma_{0\mathrm{m}}/\sqrt{3}$, etc., with $\rho_{\mathrm{f}} = \rho_{\mathrm{f}}(v_{\mathrm{f}}) \geqslant 1$ (see Taliercio, 1991).

Note that the slip surfaces defining the failure mechanisms for the RVE shown in Fig. 11 can be seen as a schematization of the localization patterns for the plastic equivalent strain inferable from Fig. 6.

The simple microscopic stress and velocity fields outlined above have the advantage of leading to analytical expressions, e.g., for the off-axis strength of the composite (Taliercio and Sagramoso, 1995). More sophisticated static and kinematic solutions were proposed, e.g., by Francescato and Pastor (1997), who numerically computed inner and outer bounds to $G^{\hom}$ using linear programming.

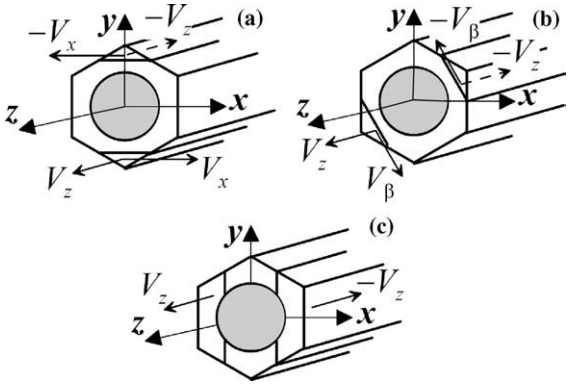

Fig. 11. Periodic failure mechanisms employed to evaluate outer bounds to the macroscopic strength domain of the composite.

References

ABAQUS Theory Manual, version 5.7, 1997. Hibbit, Karlsson & Sorensen Inc., Pawtucket, RI (USA).

Aboudi, J., 1991. Mechanics of Composite Materials: A Unified Micromechanical Approach. Elsevier, Amsterdam.

Aghdam, M.M., Pavier, M.J., Smith, D.J., 2001. Micro-mechanics of off-axis loading of metal matrix composites using finite element analysis. Int. J. Solids Struct. 38 (22–23), 3905–3925.

Benveniste, Y., 1987. A new approach to the application of Mori–Tanaka's theory in composite materials. Mech. Mater. 6, 147–157.

Brockenbrough, J.R., Suresh, S., Wienecke, H.A., 1991. Deformation of metal–matrix composites with continuous fibers: geometrical effects of fiber distribution and shape. Acta Metall. Mater. 39 (5), 735–752.

Capsoni, A., Corradi, L., 1997. A finite element formulation of the rigid-plastic limit analysis problem. Int. J. Numer. Meth. Eng. 40, 2063–2086.

Carvelli, V., Taliercio, A., 1999a. Plane strain limit analysis of fiber-reinforced periodic composites (in Italian). In: Proc. XIV Natl. Conf. of the Italian Association of Theoretical and Applied Mechanics (AIMETA), Como (I), October 6–9, 1999, 10 pp. (CD-Rom).

Carvelli, V., Taliercio, A., 1999b. A micromechanical model for the analysis of unidirectional elastoplastic composites subjected to 3D stresses. Mech. Res. Comm. 26 (5), 547–553.

Corigliano, A., 2003. Damage and fracture mechanics techniques for composite structures. In: Milne, I., Ritchie, R.O., Karihaloo, B. (Eds.), Comprehensive Structural Integrity, vol. 3. Elsevier, Oxford (UK), pp. 459–539, Chapter 9.

de Buhan, P., Taliercio, A., 1991. A homogenization approach to the yield strength of composite materials. Eur. J. Mech. A/Solids 10, 129–154.

Débordes, O., 1986. Homogenization computations in the elastic or plastic collapse range. Application to unidirectional composites and perforated sheets. In: Proc. 4th Int. Symp. Innovative Numerical Methods in Engineering, Atlanta. Springer-Verlag, pp. 453–458.

Dvorak, G.J., Bahei-El-Din, Y.A., 1979. Elastic–plastic behavior of fibrous composites. J. Mech. Phys. Solids 27, 51–72.

Dvorak, G.J., Bahei-el-Din, Y.A., Macheret, Y., Liu, C.H., 1988. An experimental study of the elastic–plastic behaviour of a fibrous boron–aluminium composite. J. Mech. Phys. Solids 36, 655–687.

Eshelby, J.D., 1957. The determination of the elastic field of an ellipsoidal inclusion, and related problems. Proc. Roy. Soc. A 241, 376–396.

Francescato, P., Pastor, J., 1997. Lower and upper numerical bounds to the off-axis strength of unidirectional fiber reinforced composites by limit analysis methods. Eur. J. Mech. A/Solids 16 (2), 213–234.

Hashin, Z., Rosen, B.W., 1964. The elastic moduli of fiber-reinforced materials. J. Appl. Mech. Trans. ASME 86, 223–232.

Hashin, Z., Shtrikman, S., 1963. A variational approach to the theory of the elastic behaviour of multiphase materials. J. Mech. Phys. Solids 11, 127–140.

Hill, R., 1965. A self-consistent mechanics of composite materials. J. Mech. Phys. Solids 13, 213–222.

Jiang, M., Jasiuk, I., Ostoja-Starzewski, M., 2002. Apparent elastic and elastoplastic behavior of periodic composites. Int. J. Solids Struct. 39 (1), 199–212.

Ju, J.W., Lee, H.K., 2001. A micromechanical damage model for effective elastoplastic behavior of partially debonded ductile matrix composites. Int. J. Solids Struct. 38 (36–37), 6307–6332.

Malkus, D.S., Hughes, T.J.R., 1978. Mixed finite element methods—reduced and selective integration techniques: a unification of concepts. Comp. Meth. Appl. Mech. Eng. 15, 63–81.

Nagtegaal, J.C., Parks, D.M., Rice, J.R., 1974. On numerically accurate finite element solutions in the fully plastic range. Comp. Meth. Appl. Mech. Eng. 4, 153–177.

Nemat-Nasser, S., Hori, M., 1993. Micromechanics: Overall Properties of Heterogeneous Materials. North-Holland, Amsterdam.

Owen, D.R.J., Hinton, E., 1980. Finite Elements in Plasticity: Theory and Practice. Pineridge Press, Swansea, UK.

Pindera, M.J., Aboudi, J., 1988. Micromechanical analysis of yielding of metal matrix composites. Int. J. Plast. 4, 195–214.

Sun, C.T., Chen, J.L., Sha, G.T., Koop, W.E., 1990. Mechanical characterization of SCS-6/Ti-6-4 metal matrix composite. J. Comp. Mater. 24, 1029–1059.

Suquet, P., 1982. Plasticity and homogenization (in French). Ph.D. thesis, Université Paris VI.

Suquet, P., 1987. Elements of homogenization for inelastic solid mechanics. In: Sanchez-Palencia, E., Zaoui, A. (Eds.), Homogenization Techniques for Composite Media, Lecture Notes in Physics, vol. 272. Springer, New York, pp. 193–278.

Taliercio, A., 1991. Role of the fiber–matrix interface in the formulation of macroscopic strength models for composite materials (in Italian). In: Proc. Natl. Conf. of the Italian Association of Theoretical and Applied Mechanics (AIMETA), Amalfi (I), June 3–5, 1991, pp. 315–324.

Taliercio, A., 1992. Lower and upper bounds to the macroscopic strength domain of a fiber reinforced composite material. Int. J. Plast. 8, 741–762.

Taliercio, A., Carvelli, V., 1999. 2D finite elements for the analysis of fiber reinforced composites subjected to 3D stresses. In: Proc. 9th European Conference on Computational Mechanics (ECCM'99), Munich (D), CD-Rom.

Taliercio, A., Coruzzi, R., 1999. Mechanical behaviour of brittle matrix composites: a homogenization approach. Int. J. Solids Struct. 36, 3591–3615.

Taliercio, A., Sagramoso, P., 1995. Uniaxial strength of polymeric–matrix fibrous composites predicted through a homogenization approach. Int. J. Solids Struct. 32, 2095–2123.

Teply, J.L., Dvorak, G.J., 1988. Bounds on overall instantaneous properties of elastic–plastic composites. J. Mech. Phys. Solids 36 (1), 29–58.

Tyrrell-Rockafellar, R., 1970. Convex Analysis. Princeton University Press, Princeton, NJ.

Xia, Z., Zhang, Y., Ellyin, F., 2003. A unified periodical boundary conditions for representative volume elements of composites and applications. Int. J. Solids Struct. 40 (8), 1907–1921.